Biophysical *Journal*
Article

Biophysical Society

Bromodomains regulate dynamic targeting of the PBAF chromatin-remodeling complex to chromatin hubs

Charles A. Kenworthy,[1] Nayem Haque,[1] Shu-Hao Liou,[1] Panagiotis Chandris,[2] Vincent Wong,[1] Patrycja Dziuba,[1] Luke D. Lavis,[3] Wei-Li Liu,[1] Robert H. Singer,[1,3] and Robert A. Coleman[1,*]

[1]Gruss-Lipper Biophotonics Center, Department of Cell Biology, Albert Einstein College of Medicine, New York; [2]Section on High Resolution Optical Imaging, National Institute on Biomedical Imaging and Bioengineering, National Institutes of Health, Bethesda, Maryland; and [3]Janelia Research Campus, Howard Hughes Medical Institute, Ashburn, Virginia

ABSTRACT Chromatin remodelers actively target arrays of acetylated nucleosomes at select enhancers and promoters to facilitate or shut down the repeated recruitment of RNA polymerase II during transcriptional bursting. It is poorly understood how chromatin remodelers such as PBAF dynamically target different chromatin states inside a live cell. Our live-cell single-molecule fluorescence microscopy study reveals chromatin hubs throughout the nucleus where PBAF rapidly cycles on and off the genome. Deletion of PBAF's bromodomains impairs targeting and stable engagement of chromatin in hubs. Dual color imaging reveals that PBAF targets both euchromatic and heterochromatic hubs with distinct genome-binding kinetic profiles that mimic chromatin stability. Removal of PBAF's bromodomains stabilizes H3.3 binding within chromatin, indicating that bromodomains may play a direct role in remodeling of the nucleosome. Our data suggests that PBAF's dynamic bromodomain-mediated engagement of a nucleosome may reflect the chromatin-remodeling potential of differentially bound chromatin states.

SIGNIFICANCE Transcriptional bursting involves a gene rapidly switching between transcriptionally active and inactive states. To regulate transcriptional bursting, chromatin must interchange between euchromatin and heterochromatin to permit or restrict access of transcription factors including RNA polymerase II to enhancer and gene promoters. However, little is known regarding how chromatin remodelers dynamically read a rapidly changing 4D epigenome. We used live-cell single-molecule imaging to characterize the spatiotemporal chromatin-binding dynamics of PBAF, a chromatin remodeler that accesses both euchromatin and heterochromatin to regulate transcription. PBAF cycles on and off chromatin hubs in select nuclear regions where it distinctly engages euchromatin and heterochromatin via bromodomains in its BAF180 subunit. Our study provides the framework to understand how the 4D epigenome is regulated.

INTRODUCTION

Transcriptional bursting is defined by brief periods of time where a gene promoter is in a highly permissible state that allows transcription-factor recruitment and rapid loading of RNA polymerase II (RNA Pol II) every 8–20 s (1). After a period of minutes, the gene is shut down and transcriptionally silent for a period of minutes to hours (2). There is a tight linkage between transcriptional activity and chromatin-state changes such as the interconversion between euchromatin and heterochromatin (3). Therefore, it is likely that chromatin remodelers (e.g., PBAF), histone variants (e.g., H3.3), and factors that actively stabilize different chromatin states (e.g., H1/HP1α) also bind and unbind enhancers and promoters in a cyclical manner (4–6).

Recent live-cell imaging studies indicate that transcription factors (e.g. RNA Pol II, mediator, and Sox2) dynamically bind chromatin as clusters to form hubs of activity that regulate local gene expression (7–12). However, such dynamic activity of chromatin modifiers within distinct chromatin hubs is currently poorly characterized due to a number of technical limitations. In particular, researchers lack efficient methods to identify and quantitatively characterize chromatin in active/inactive hubs in live cells.

Submitted July 23, 2021, and accepted for publication March 24, 2022.

*Correspondence: robert.coleman2@einsteinmed.edu

Wei-Li Liu is deceased.

Editor: Yi Qin Gao.

https://doi.org/10.1016/j.bpj.2022.03.027

© 2022 Biophysical Society.

This is an open access article under the CC BY-NC-ND license (http://creativecommons.org/licenses/by-nc-nd/4.0/).

PBAF is an ATP-dependent chromatin-remodeling complex that both evicts or repositions nucleosomes to regulate transcription of stress-response genes via bromodomain-dependent targeting of acetylated chromatin (13–15). Numerous in vitro studies have found that the removal or mutational inactivation of bromodomains in the BAF180 subunit reduces PBAF's binding to chromatin (16,17). However, none of these studies determined if bromodomains regulate both the association and dissociation of PBAF with acetylated chromatin in vivo. In addition, PBAF targets heterochromatin to actively repress transcription likely via repositioning or stabilizing a nucleosome at promoters and enhancers through a poorly characterized mechanism (18–21). Therefore, understanding how PBAF dynamically recognizes highly localized hubs of different chromatin states may lead to a greater understanding of the spatial and dynamic regulation of chromatin topology and gene regulation in vivo.

To spatially distinguish and characterize different types of chromatin hubs in vivo, we used live-cell single-molecule tracking (SMT) to dynamically map chromatin binding of PBAF alongside prototypical markers of euchromatin (H3.3) and heterochromatin (HP1α). Our dynamic imaging studies reveal small hubs where PBAF cycles on and off chromatin. To map out different chromatin states, we investigated PBAF's engagement and stability on chromatin when encountering H3.3- and HP1α-marked hubs. More importantly, we assessed the role of PBAF's bromodomains in guiding PBAF to nuclear hubs and influencing PBAFs ability to selectively engage euchromatic and heterochromatic hubs. Overall, our studies provide new insights into dynamic chromatin targeting of PBAF via bromodomains.

MATERIALS AND METHODS

Plasmid constructions, generation of cell lines, and live-cell fluorescent labeling of proteins

Details of plasmid construction, generation of cell lines, and fluorescent labeling of proteins are described in the supplemental experimental procedures.

Live-cell single-molecule imaging of Halo-BAF180 wild-type (WT)/ΔBD, H3.3-SNAP, or SNAP-HP1α

All imaging sessions were carried out at room temperature in L-15 media (Gibco, Waltham, MA) to support cell growth in conditions lacking CO_2. Experiments were performed at room temperature to minimize microscope drift and cell movement, which can substantially affect identification of hubs. Imaging experiments performed at 37°C showed equivalent residence times and distributions of Halo-BAF180 compared with imaging performed at room temperature, with the exception that the residence time of PBAF binding state 3 was decreased at 37°C (Fig. S9 *A*). In addition, the ratio of binding events inside hubs compared with outside of hubs was substantially lower at 37°C compared with at 25°C (Fig. S9 *B*), likely due to cell movement or stage drift, which makes hub identification more difficult. Cells were continuously illuminated using a 532 nm (13 W/cm^2, Coherent, Santa Clara, CA) or 640 nm (9.5 W/cm^2, Coherent) laser for JF549-HTL and SNAP-Cell 647-SiR imaging, respectively. Time-lapse two-dimensional (2D) images of single molecules were acquired with a customized inverted Nikon Eclipse Ti microscope with a 100× oil-immersion objective lens (1.49 NA, Nikon, Melville, NY) and were further magnified 1.9× post-objective. BAF180 images were acquired at 2 Hz for ∼18 min using an EMCCD (iXon, Andor, Belfast, UK) with a 512 × 512 pixel field of view (final pixel size of 84 nm). SNAP imaging proceeded at 2 Hz for ∼4.5 min in cells that expressed either SNAP-Cell 647-SiR-labeled H3.3-SNAP or SNAP-HP1α.

Image processing and SMT

Movies of acquired images were processed to subtract background in ImageJ using a rolling ball radius of 50 pixels. Background subtracted movies were subjected to multi-target tracking to resolve the trajectories of individual molecules (22) using a GUI-based implementation, SLIMfast (23). Localization of individual molecules was achieved by fitting point spread functions (PSFs) of discrete single spots with a 2D Gaussian function. Tracking of single-molecule chromatin-binding events was performed by connecting BAF180 localizations between consecutive frames. Tracking was based upon a maximum expected diffusion constant of 0.05 μm^2/s and allowed for 1.5 s gaps in trajectories due to blinking or missed localizations. A 2D projection map of BAF180-binding events was generated by determining the average *x*,*y* position from each individual binding trajectory acquired over 18 min of imaging.

Nuclear BAF180 tracks were identified based on the boundaries from 2D projection maps of 180 binding events. BAF180 tracks that fell outside of the nucleus were excluded. Photobleach rates were then determined for each background-subtracted movie based upon exponential decay of the global fluorescence of chromatin-bound Halo-BAF180 WT/ΔBD, H3.3-SNAP, or SNAP-HP1α.

Analysis of PBAF chromatin-binding residence times

Chromatin-binding residence times were determined by plotting a survival curve (1-cumulative density function [1-CDF]) of the track lengths of chromatin-bound Halo-BAF180 in each cell. Single- and double exponential models were then fitted to these 1-CDF plots to determine residence times. Residence times were photobleach corrected as previously described (24). One-way analysis of variance followed by Tukey's post hoc *t*-tests were performed to determine pairwise significance of global residence times and percentages of stable PBAF binding events.

GRID analysis was performed on residence times aggregated from multiple cells using a regularization parameter of 0.05 and kmin/kmax values of -3 and 1, respectively, for all conditions. Fits were resampled 100 times containing 80% of the data to obtain mean and error values. Statistical significance was determined using a two tailed Student's *t*-test.

Analysis of PBAF clustering in hubs

2D projection maps of BAF180-binding events lasting at least 1 (Fig. 2 *B*) or 8 s (Fig. S4 *B*) were expanded 10-fold in the *x* and *y* directions, yielding a final pixel size of 8.4 nm. Areas of high PBAF binding densities were determined by counting the number of binding events within an octagon window (diameter: 168 nm) as it was raster scanned across the nucleus of the expanded 2D projection map. Contiguous octagon widows centered on an individual pixel containing at least 3 PBAF binding events were defined and labeled as hubs. The total number of hubs per cell were then normalized to the total PBAF binding events per cell and multiplied to produce the number of PBAF hubs formed per 10,000 PBAF binding events

(i.e., number of PBAF hubs) for each cell. The median number of PBAF binding events inside hubs in cells was also normalized to the total PBAF binding events per cell and multiplied to produce the number of PBAF binding events in hubs per 10,000 PBAF binding events over 18 min of imaging. Overall significance was determined with a two-sample Kruskal-Wallis test to determine pairwise significance.

Characterization of PBAF localization and binding dynamics in proximity to H3.3 or HP1α hubs

High-binding density H3.3 or HP1α hubs were mapped using multi-target tracking and raster scanning as described above. Track lengths for PBAF molecules within hubs whose centroids were within 500 nm of H3.3 or HP1α hub centroids were aggregated from a number of cells and plotted as a 1-CDF survival curve and fit to single- and double exponential decay functions. The proximity distance of 500 nm was chosen to reflect the size of the hubs (∼200–400 nm diameter) and the close association of PBAF with H3.3 or HP1α as seen in our fixed-cell STORM microscopy experiments (Fig. S8). Residence times of the specific binding population for PBAF in co-localized hubs were plotted as a 1−CDF plot. Statistical differences between genotype or treatment conditions were then assessed using a two-sample Kolmogorov-Smirnov test.

RESULTS

PBAF targets chromatin in distinct nuclear hubs and compartments

A number of prior studies found that transcription factors, including EWS/FLI, Sox 2, and RNA Pol II, along with histones, formed highly localized clusters or hubs of binding in enhancers or promoters within nuclear domains of ∼200–300 nm in diameter (8,9,11,25). However, the molecular origins of dynamic transcription-factor binding on chromatin hubs is poorly understood. Therefore, we chose to study how the cycling of factors on and off of chromatin on the timescale of seconds to minutes is influenced by histone post-translational modifications (PTMs) and chromatin subtypes (e.g., euchromatin versus heterochromatin).

Enhancers and promoters of transcriptionally active genes are enriched in acetylated chromatin (26). Accordingly, we hypothesized that chromatin remodelers such as PBAF, which targets a variety of acetylated residues via its 8–14 bromodomains (18,27), would also form dynamic binding hubs in the nucleus (Fig. 1 *A*). To characterize the dynamic binding of PBAF to chromatin in vivo, we chose to fluorescently tag the BAF180 subunit (i.e., Halo-BAF180 WT; Fig. S1), since it is present as two copies within PBAF and harbors six bromodomains/copy that are critical for interaction with acetyl-lysine residues on histones (16,17). We confirmed that these Halo-tagged BAF180 proteins were incorporated into the large multi-subunit PBAF complex via co-immunoprecipitation studies and live-cell fast-diffusion measurements (Figs. S1 and S2; Videos S6 and S7). Quantitative analysis of Western blots from nuclear extracts revealed that nuclear Halo-BAF180 WT is not overexpressed relative to the endogenous BAF180 in a U2OS cell line expressing the Halo tag alone (Fig. S1 *C* and *D*). This is likely due to the fact that overexpressed subunits that are not incorporated into multi-subunit complexes are often degraded (28).

Motion-blur HILO microscopy combined with live-cell SMT was used to detect fluorescent PBAF molecules that were bound to chromatin (Fig. 1 *B*; Video S1) (24). At long camera exposure rates (∼500 ms), fast-diffusing nuclear PBAF complexes are blurred out and cannot be localized (24). Single PBAF molecules, stably bound to chromatin, appear as distinct PSFs that are spatially and temporally resolved (Fig. 1 *B*) (24). PSFs, representing PBAF's binding and unbinding on chromatin, appear and disappear stochastically throughout the time course of imaging (Fig. 1 *B*; Video S1). 2D projection maps showed select nuclear regions that contained high densities of PBAF chromatin-binding events (Figs. 1 *C* and S3 *C*). Pair correlation function analysis, which was previously used for determination of transcription-factor clustering (9), found that PBAF formed binding hubs of ∼200–400 nm in diameter (Fig. S3 *D*).

To better identify and quantify PBAF's dynamic binding in chromatin hubs, we developed an approach to spatially define the frequency of PBAF's chromatin binding within nuclear subregions. Individual pixels in these dynamic binding-frequency heatmaps were calculated by raster scanning across the nucleus and counting the number of PBAF chromatin-binding events in a window of approximately 252 nm diameters as the window was raster scanned across the nucleus (Fig. 1 *C* and *D*). Spatially isolated regions spanning ∼200–400 nm in diameter representing high-frequency PBAF binding to chromatin were scattered throughout the nucleus (Fig. 1 *D*). No hubs were detected in simulations with random localizations of an equivalent number of binding events throughout the nucleus for every cell included in our analysis (see Fig. S4 *A* for a representative cell). Based upon PBAF's known role in remodeling chromatin in genomic elements associated with transcriptional regulation, we hypothesized that PBAF's binding in equivalently sized hubs as Sox2 and RNA Pol II was due, in part, to dynamic interactions with chromatin in enhancers and promoters.

PBAF targeting to chromatin hubs is regulated by BAF180 bromodomains

Histone PTMs associated with transcriptional regulation (e.g., acetylation) are ideal targets to better understand the molecular origins of PBAF cycling on chromatin hubs. Therefore, we chose to see how disruption of PBAF's interaction with histone PTMs affected targeting to chromatin hubs. Arrays of acetylated nucleosomes can be repeatedly targeted by bromodomain containing chromatin-remodeling complexes such as PBAF (Fig. 2 *A*) (29). BAF180's six bromodomains allow PBAF to recognize a large variety of acetyl-lysine residues in chromatin (27,30–32). Therefore, we compared the high-frequency binding of a WT PBAF

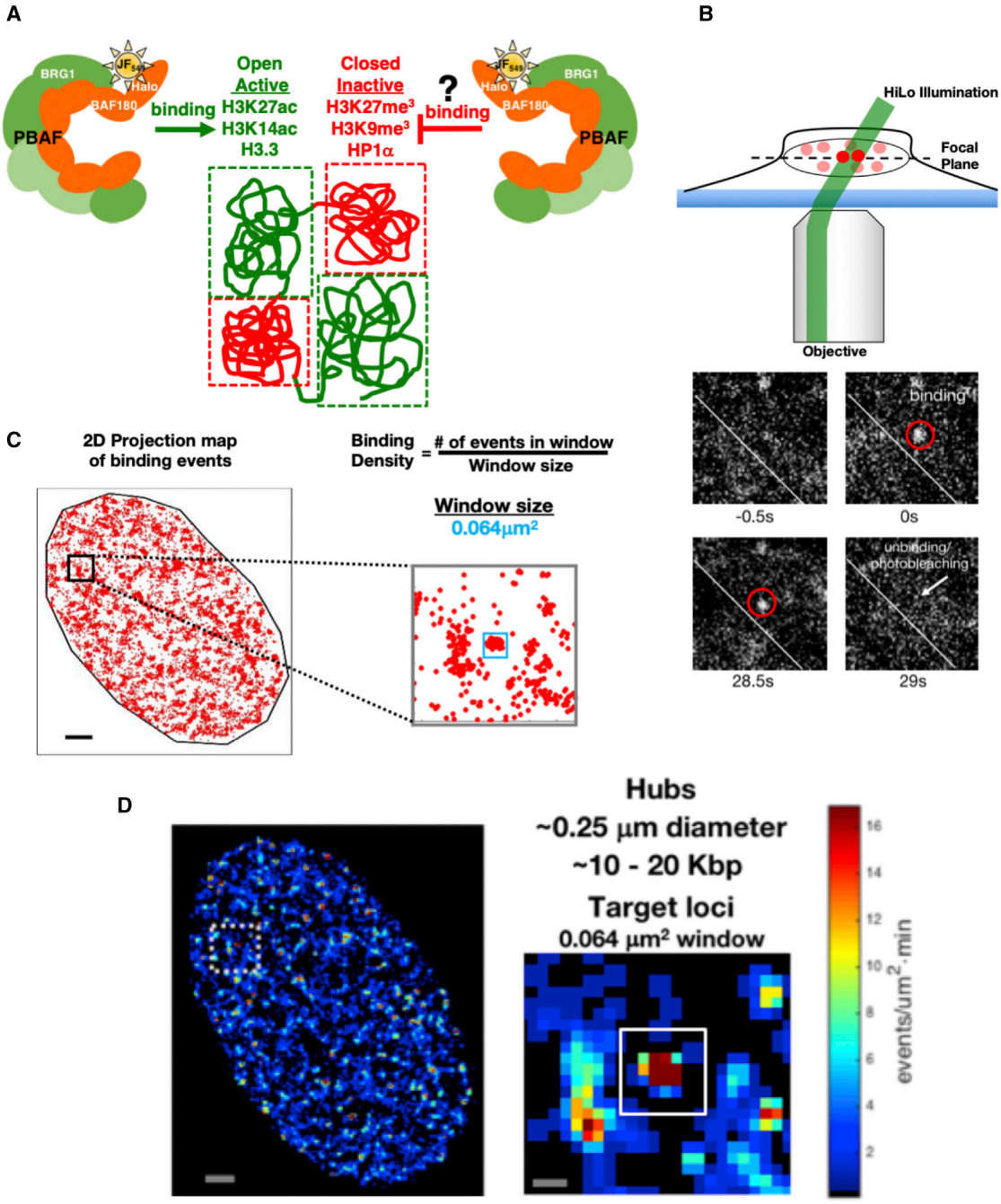

FIGURE 1 Spatial analysis of PBAF chromatin-binding events using SMT to define binding hubs. (*A*) Transcriptionally active genomic regions (green) contain open chromatin structures associated with acetylated histone marks (e.g., H3K27ac and H3K14ac) and the H3.3 histone variant. Transcriptionally inactive genomic regions (*red*) contain closed chromatin structures associated with select methylated histone marks (e.g., H3K27me^3 and H3K9me^3) and heterochromatic protein HP1α. PBAF contains multiple bromodomains within the BAF180 subunit known to bind acetylated histone marks associated with open chromatin regions. (*B*) Motion-blur HiLo microscopy (*top panel*) of a single U2OS cell stably expressing Halo-BAF180 WT. PBAF containing Halo-BAF180 WT molecules that rapidly diffuse in the nucleoplasm are blurred, while chromatin-bound PBAF appears as single bright spots (*highlighted by red circles*, *lower panels*). Disappearance of a spot (white arrow) is due to unbinding or dissociation of PBAF from the chromatin. A diagonal white line is an added spatial reference that is positioned at the same location in each frame. (*C*) Strategy for measuring the non-homogeneous localization of PBAF chromatin-binding events in a nucleus. A 2D projection map of PBAF binding events (red dots) in the nucleus over 18 min of imaging is shown. A gray box (*left panel*, *zoomed view in the right panel*) outlines a representative window of PBAF binding events in a subnuclear region. PBAF binding density is thereby determined by counting the number of binding events located within a given size window (0.064 μm^2, *blue box*). Scale bar, 2 μm. (*D*) PBAF binding-event-frequency heatmaps were obtained using the 2D projection map in (*C*). Regions of high (*red*) and low (*blue*) PBAF binding frequency are presented for the cell shown in (*C*). The right panel is a zoomed in view of the dashed box in left panel. PBAF hubs (*right panel*, *white box*) were identified as clusters of frequent PBAF chromatin binding to target loci. Scale bar, 2 μm (*left panel*) and 0.25 μm (*right panel*), respectively. To see this figure in color, go online.

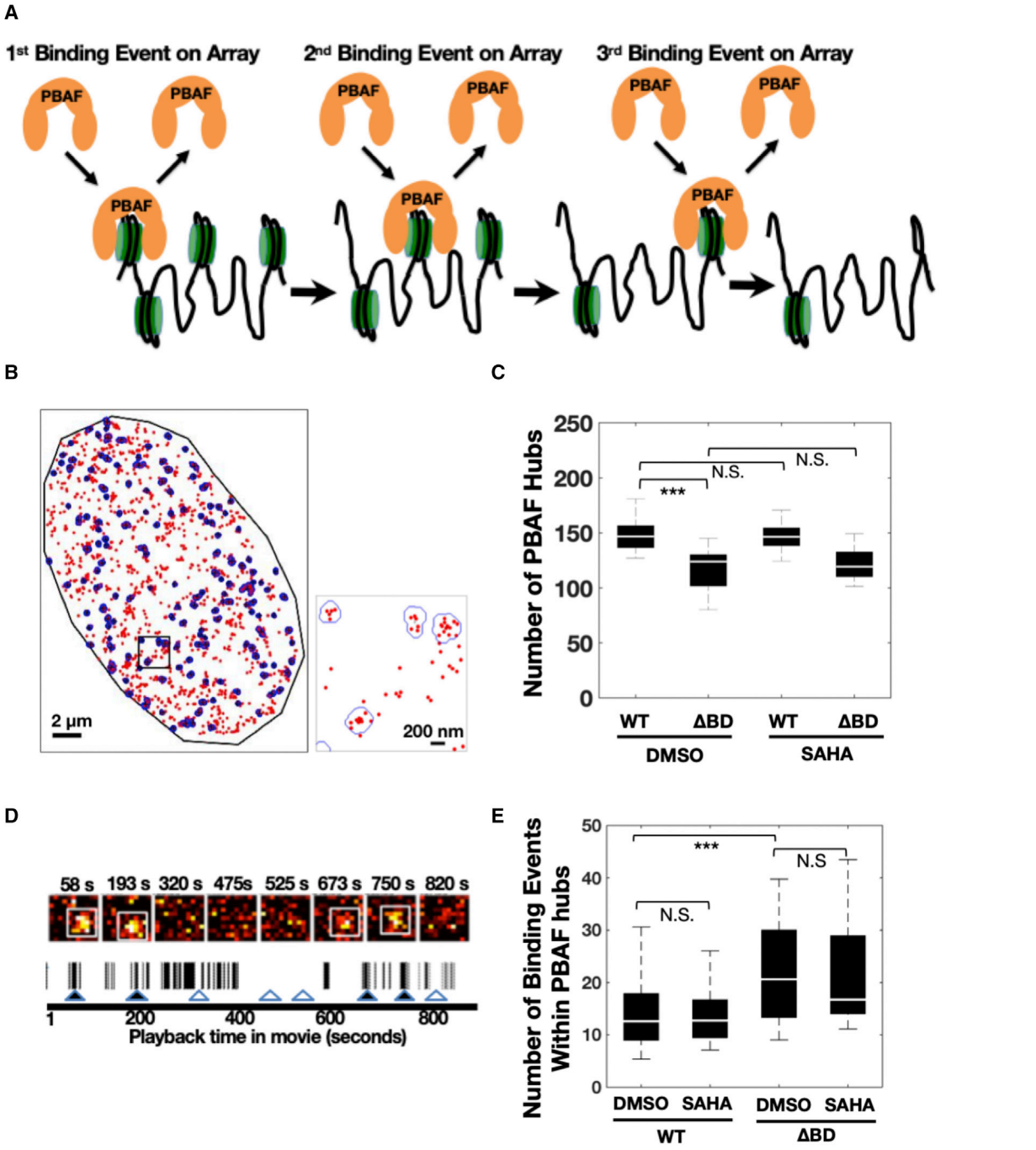

FIGURE 2 Spatial and cycling analysis of PBAF binding hubs. (*A*) A schematic representation where PBAF cycles on and off an array of nucleosomes. (*B*) Clustering analysis algorithms indicate PBAF binding events (*red dots*) within hubs (*left panel*, *blue outlines*). The right panel displays an expanded inset of a boxed region in the left panel. (*C*) The number of hubs formed per cell, which express either PBAF WT or the mutant PBAF ΔBD. (*D*) Temporal occupancy of PBAF at a representative chromatin-binding hub. Snapshots of PBAF binding foci at different time points in movie (seconds) and the appearance of PBAF binding highlighted by white boxes (*top panel*). The width of the black bars represents the duration of individual PBAF/chromatin-binding events in a hub (*bottom panel*). White gaps represent latent time periods when the region containing a hub is not occupied by PBAF. Timepoints (▲) from the top panel where PBAF binds in the hub. Timepoints (Δ) where PBAF does not bind the hub. (*E*) Median number of PBAF binding events per hub per cell accumulated over an 18 min time window ($N = 39$ WT DMSO cells, 17 ΔBD DMSO cells, 37 WT suberoylanilide hydroxamic acid [SAHA] cells, and 21 ΔBD SAHA cells). N.S., not significant, and ***$p < 0.001$. For data in (*C*), and (*E*), the white bar in the solid black box is the median, while the lower and upper boundaries of the black box correspond to the 25th and 75th percentiles of the data, respectively. Outliers typically represented less than 10% of the dataset and therefore were omitted for clarity. To see this figure in color, go online.

and a mutant PBAF lacking the six BAF180 bromodomains (i.e., ΔBD) (Figs. 2 *B* and S1 *A*).

Many transcription factors, chromatin remodelers, and replication factors exhibit transient interactions (<1 s) with chromatin (24,28,33). Transient and likely non-specific probing of PBAF on chromatin could generate background noise that impairs hub detection. Thus, we limited our analysis to PBAF chromatin-binding events lasting longer than 1 s. The number of PBAF binding hubs in each cell was reduced upon deletion of BAF180 bromodomains (Fig. 2 *C*). We did not see a significant change in the number of WT or ΔBD PBAF binding hubs when global levels of histone acetylation were elevated via SAHA treatment (Figs. 2 *C* and S4 *B*). However, the number of WT PBAF binding hubs increased in a BAF180 bromodomain-dependent manner upon histone hyperacetylation when filtering the data to only include binding events greater than 8 s (Fig. S4 *C*). This suggests that histone hyperacetylation contributes to increased PBAF target-hub selection, but this may be dictated by enhanced stability of PBAF on chromatin in hubs.

Of note, removal of BAF180 bromodomains only weakened, but did not completely eliminate, ΔBD PBAF's ability to bind chromatin hubs. This suggests that only a subset of target chromatin hubs are dependent on BAF180 bromodomains. Alternatively, additional chromatin-binding domains (e.g., bromodomains, BAH, and PHD) in other PBAF subunits compensate for the removal of BAF180 bromodomains. Overall, our data indicate that at least a subset of target hubs are defined by repeated rounds of PBAF binding to chromatin via BAF180 bromodomains/acetyl-lysine interactions.

BAF180 bromodomains do not inherently promote more frequent cycling of PBAF on chromatin in hubs

Our data thus far indicated that bromodomain/acetyl-lysine interactions in nucleosomes may strengthen PBAF's binding to chromatin, consistent with previous in vitro biochemical studies (16,17,34). However, prior studies did not address if bromodomain/acetylated histone contacts increased the association (k_{on}) or decreased the dissociation (k_{off}) of PBAF binding to chromatin in vivo. We took multiple approaches to answer this question. To analyze PBAF's association with chromatin, we investigated PBAF cycling rates on chromatin in target hubs. Chromatin hubs are occupied via a series of PBAF binding and unbinding events interspersed with latent periods of non-occupancy (Fig. 2 *D*). If BAF180 bromodomain/acetylated histone interactions directly promoted faster association (e.g., increased k_{on}) of PBAF with chromatin, histone hyperacetylation should increase WT PBAF's cycling rates on chromatin. Histone hyperacetylation did not significantly impact cycling rates of WT or ΔBD PBAF on chromatin in hubs (Fig. 2 *E*). This indicates the histone hyperacetylation likely only increases the number of chromatin targets that are more stably bound by PBAF's BAF180 bromodomains (Fig. S4 *C*) while having little effect on promoting faster association with acetylated chromatin.

In addition, ΔBD PBAF should cycle less frequently on chromatin hubs compared with WT PBAF if BAF180 bromodomain/histone acetylation interactions promoted faster association (e.g., increased k_{on}) with acetylated chromatin. In stark contrast to this idea, ΔBD PBAF exhibited more rounds of repeated binding events on hubs compared with WT PBAF (Fig. 2 *E*). It is important to note that the number of PBAF binding events in the WT and ΔBD PBAF hubs was acquired over an 18 min time window and was normalized to the total number of binding events in each cell. Also, WT and ΔBD PBAF hubs are approximately the same size, suggesting that ΔBD PBAF cycles faster than WT PBAF. Overall, differences in cycling rates between WT and ΔBD PBAF indicate that the time-dependent fluctuation of fluorescent signals in hubs is not due to inherent blinking of the dye, which should be independent of the protein that is labeled. Rather, cycling of PBAF on and off chromatin hubs on the timescale of seconds to minutes is likely due to repeated rounds of binding and unbinding to chromatin.

The increased cycling rate of ΔBD PBAF on chromatin may be due to mass-action effects since removal of BAF180 bromodomains allows ΔBD PBAF to target only a limited subset of chromatin hubs. In other terms, WT PBAF cycles less frequently on chromatin since it has more potential hub targets, essentially diluting out the concentration of PBAF available for re-visiting. Alternatively, ΔBD PBAF could bind chromatin for shorter periods of time, effectively increasing the concentration of freely diffusing PBAF relative to WT PBAF. Consistent with this alternative mechanism, the number of hubs targeted by ΔBD PBAF only decreases 16%, while cycling frequency increases by 39%, compared with WT PBAF. Thus, our data supports that BAF180 bromodomains do not promote faster association of PBAF with acetylated chromatin.

PBAF stably engages chromatin in hubs via BAF180 bromodomains

In vitro biochemical experiments indicate that PBAF mobilizes/evicts nucleosomes via a multi-step pathway that likely involves an initial transient encounter with a nucleosome (state 1), a stable nucleosome engagement (state 2), and an ATP-dependent DNA translocation that can lead to nucleosome mobilization or eviction (states 3–4) followed by dissociation of PBAF from the DNA scaffold (Fig. 3 *A*) (34–36). Based upon this mechanism, BAF180 bromodomains could promote efficient stable engagement of acetylated chromatin (e.g., transition from state 1 to 2). SMT is a powerful technique that measures kinetic parameters of

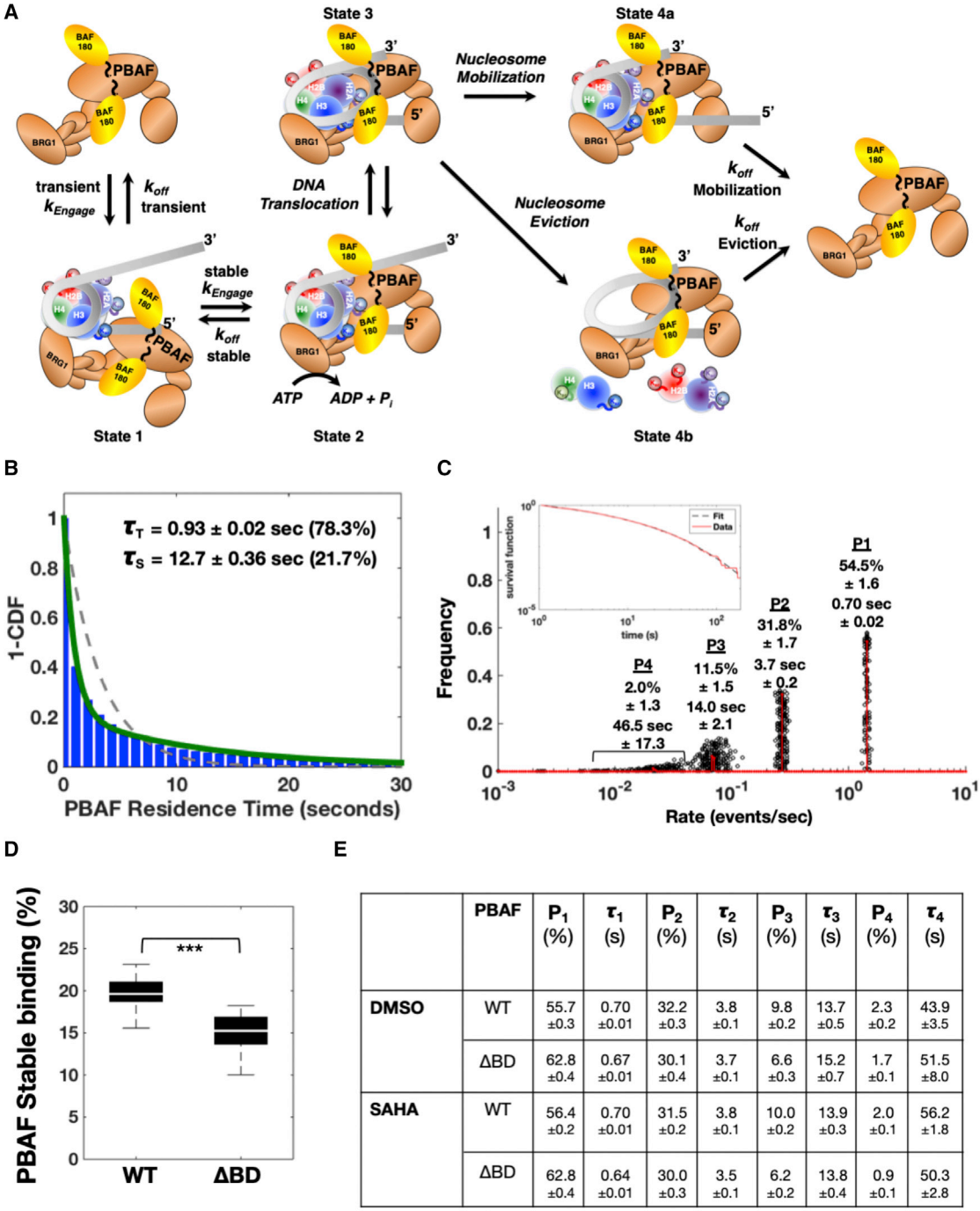

E

	PBAF	P_1 (%)	τ_1 (s)	P_2 (%)	τ_2 (s)	P_3 (%)	τ_3 (s)	P_4 (%)	τ_4 (s)
DMSO	WT	55.7 ±0.3	0.70 ±0.01	32.2 ±0.3	3.8 ±0.1	9.8 ±0.2	13.7 ±0.5	2.3 ±0.2	43.9 ±3.5
	ΔBD	62.8 ±0.4	0.67 ±0.01	30.1 ±0.4	3.7 ±0.1	6.6 ±0.3	15.2 ±0.7	1.7 ±0.1	51.5 ±8.0
SAHA	WT	56.4 ±0.2	0.70 ±0.01	31.5 ±0.2	3.8 ±0.1	10.0 ±0.2	13.9 ±0.3	2.0 ±0.1	56.2 ±1.8
	ΔBD	62.8 ±0.4	0.64 ±0.01	30.0 ±0.3	3.5 ±0.1	6.2 ±0.2	13.8 ±0.4	0.9 ±0.1	50.3 ±2.8

FIGURE 3 Spatial analysis of PBAF's stability on chromatin. (*A*) A schematic showing kinetic mechanism for PBAF binding and remodeling of a nucleosome. (*B*) 1-cumulative distribution function (1-CDF) plot of WT PBAF's chromatin-binding residence time inside hubs in a cell. 1-CDF plots were fitted to a single (*dashed gray*) and double (*solid green*) exponential-decay model. The residence time (τ) and its corresponding percentage for each population (i.e., transient [T] and stable [S]) are indicated. $N = 7662$ PBAF binding events in hubs in cell. (*C*) GRID analysis of WT PBAF's chromatin-binding τ inside hubs in same cell as (*B*). (*D*) Median percentage of Halo-BAF180 WT or Halo-BAF180 ΔBD (ΔBD) binding events displaying stable (S, >1 s binding) binding to chromatin inside and outside of hubs ($N = 39$ WT DMSO cells, 17 ΔBD DMSO cells) as determined by fitting using a double exponential-decay model. (*E*) Table of GRID analysis of WT and ΔBD PBAF's chromatin-binding τ inside hubs aggregated across all cells ($N = 296{,}518$ PBAF binding events in 39 WT DMSO cells, $N = 76{,}393$ PBAF binding events in 17 ΔBD DMSO cells, $N = 326{,}102$ PBAF binding events in 37 WT SAHA cells, $N = 123{,}521$ PBAF binding events in 21 ΔBD SAHA cells). For data shown in (*D*), the white bar in the solid black box is the median, while the lower and upper boundaries of the black box correspond to the 25th and 75th percentiles of the data, respectively. N.S., not significant, and ***$p < 0.001$. Outliers typically represented less than 10% of the dataset and therefore were omitted for clarity. To see this figure in color, go online.

different populations of chromatin-bound factors (9,24,37). Therefore, we analyzed PBAF's chromatin-binding residence times within hubs. Histograms of PBAF's chromatin-binding residence times inside of hubs fit much better to a double compared with a single exponential-decay model (Fig. 3 *B*). Residence times were corrected for photobleaching (3). The predominant PBAF population (80% of molecules) transiently (<1 s) bound chromatin inside of hubs for 0.94 s (Figs. 3 *B* and S5). Transiently bound PBAF most likely represents non-specific or non-productive binding (Fig. 3 *A*, state 1), as seen previously with many other transcription factors, chromatin remodelers, and DNA-replication factors (24,28,33). The remaining PBAF molecules (20%) stably bound chromatin (>1 s) inside hubs for 12.7 s, further highlighting PBAF's dynamic interaction with chromatin (Fig. 3 *B*). Importantly, PBAF's stable residence time on chromatin (12.7 s) is significantly shorter than dye photobleaching rates ($t_{1/2}$ of approximately 60–200 s), indicating that these imaging conditions measure dissociation of PBAF from chromatin.

PBAF and ATP-dependent chromatin remodelers often act via complex multi-step kinetic pathways (Fig. 3 *A*) (35,36). Therefore, it was possible that fitting of the residence time histogram using a double exponential-decay model underestimated the number of different states of PBAF bound to chromatin in hubs. To examine for additional chromatin-bound states of PBAF, we further analyzed PBAF's residence time within hubs using GRID, which has been previously used to define multiple populations (5,6) of chromatin-bound transcription factors (38,39). GRID analysis revealed three well-defined populations and a fourth less-well-defined population of WT PBAF bound to chromatin in hubs with residence times ranging from ~0.7–50 s (Fig. 3 *C*).

To determine if BAF180 bromodomains promote stable association with acetylated chromatin, we compared WT and ΔBD PBAF's chromatin-binding residence times inside of hubs. Removal of BAF180's bromodomains (ΔBD PBAF) decreased the percentage of PBAF molecules displaying stable binding (>1 s) inside hubs (Fig. 3 *D* and *E*). While BAF180 bromodomains are not absolutely required for PBAF's interaction with chromatin, BAF180 bromodomains enhance the efficiency of PBAF's stable engagement (populations >1 s binding) with acetylated chromatin (Fig. 3 *A*, transition from state 1 to 2).

Residence times within a population of molecules that are stably bound to chromatin directly reflect dissociation rates of PBAF from a nucleosome. To determine if BAF180 bromodomains decreased the dissociation rates (e.g., k_{off}) of PBAF from chromatin, we compared the residence times of WT and ΔBD PBAF inside hubs. WT PBAF displayed longer stable residence times on chromatin compared with ΔBD PBAF via fitting with a double exponential-decay model (Fig. S5 *C*). However, GRID analysis indicated much more complicated kinetic profiles. To further characterize PBAF's longest-lived population (population 4 [P4]) that was less well defined in single cells (Fig. 3 *C*), we aggregated binding events from all cells. The residence times of ΔBD PBAF increased compared with WT PBAF at the two longest-lived populations (P3 $p < 0.0001$ and P4 $p < 0.001$) under basal levels of histone acetylation (Fig. 3 *E*). The percentage of long-lived PBAF chromatin-binding events (P3/P4) was significantly decreased upon removal of BAF180 bromodomains under basal levels of histone acetylation (Fig. 3 *E*). This decrease in the apparent residence time of ΔBD PBAF seen by fitting with the double exponential-decay model was likely due to the reduced percentage of the longest-lived PBAF populations (P3/4) upon BAF180 bromodomain removal. This highlights the importance of performing GRID analysis for chromatin-binding factors with complex kinetic profiles. Our data obtained via a more sophisticated fitting method (e.g., GRID) indicates that BAF180 bromodomains increase the percentage of PBAF binding events engaging in long-lived binding (>~13 s, P3/P4) on chromatin but does not increase PBAF's residence time on chromatin under basal levels of histone acetylation (Fig. 3 *A*, $k_{off\ stable/mobilization/eviction}$).

Hyperacetylation of histones (suberoylanilide hydroxamic acid treatment) did not significantly increase the percentage of stable chromatin-binding events of WT or ΔBD PBAF inside hubs (Fig. 3 *E*). This suggests that histone hyperacetylation does not further increase the efficiency of stable engagement of chromatin (Fig. 3 *A*, transition from state 1 to 2). Histone hyperacetylation increases the residence time of WT PBAF once fully engaged on a nucleosome, which was particularly evident on the longest-lived state (P4) in the GRID analysis (Fig. 3 *E*). Importantly, no increase in ΔBD PBAF's residence time was seen in either the double exponential-decay model or GRID analysis (Figs. S5 *C* and 3 *E*). Therefore, histone hyperacetylation allows PBAF to find new target hubs in global chromatin (Fig. S4 *B*) and further stabilizes PBAF once bound to a nucleosome (Fig. 3 *A*, states 3/4).

Chromatin inside and outside of hubs are distinct interaction scaffolds for PBAF

Chromatin hubs likely contain histone PTMs that better promote PBAF's binding to nucleosomes relative to global chromatin. To test this hypothesis, we compared kinetic profiles of PBAF's chromatin-binding residence times inside and outside of hubs. Indeed, the percentage of PBAF molecules transiently engaged (<1 s) with chromatin increased precipitously outside compared with inside hubs, with both the double exponential-decay model and GRID analysis (compare Figs. 3 *E* and S5A). This suggests that chromatin in target hubs is likely decorated with distinct histone PTMs or exists in unique structures to promote the efficiency of PBAF's stable engagement of a nucleosome compared with global chromatin outside of hubs.

Global chromatin outside of hubs could also present a unique scaffold that affects PBAF's stability on chromatin. Therefore, we compared WT PBAF's stable chromatin-binding residence time outside and inside hubs. WT PBAF's stable chromatin-binding residence time (e.g., for populations with residence times >1 s) increases outside of hubs relative to inside of hubs, as seen by both the double exponential-decay model and GRID analysis (compare Figs. 3 *E* and S5 *C*, S6 *B*, and *C*). Overall, our data suggest that WT PBAF's engagement is inefficient on global chromatin. However, once WT PBAF efficiently binds a nucleosome on global chromatin, it is stabilized via unique histone PTMs and/or structures. This further suggests that chromatin inside and outside of hubs present unique scaffolds that regulate WT PBAF's engagement and binding stability on a nucleosome.

Our data from inside chromatin hubs suggested that BAF180 bromodomains promoted efficient engagement (>1 s binding) on chromatin containing basal levels of acetylation and increased PBAF's residence time on hyperacetylated chromatin (Fig. 3 *D* and *E*). To further determine how BAF180 bromodomains impacted PBAF's stable interaction with global chromatin, we compared WT and ΔBD PBAF's kinetic binding profiles on chromatin outside of hubs. With GRID analysis, similar to what is seen inside of hubs, removal of BAF180 bromodomains further decreases PBAF's stable engagement of chromatin (percentage of binding events >1 s) outside of hubs (Fig. S6 *C*). Once PBAF is engaged on chromatin, removal of BAF180 bromodomains increases its residence time on chromatin containing basal levels of acetylation, as seen by GRID analysis (Fig. S6 *C*). Upon histone hyperacetylation, removal of BAF180 bromodomains decreases PBAF's residence time of the longest-lived populations (P3/P4) on chromatin outside of hubs (Fig. S6 *C*). Overall, our data suggest that global chromatin is also acetylated, albeit likely to some lesser degree compared with chromatin in hubs (see discussion).

Prototypical markers for euchromatin (H3.3) and heterochromatin (HP1α) form dynamic hubs

Previous studies have established that PBAF binds nucleosomes at promoters of both transcriptionally active and repressed genes (18,19,40–42). To better understand the different chromatin structures that PBAF targets in hubs, we dynamically mapped nuclear subregions associated with prototypical markers of euchromatin (H3.3-SNAP) and heterochromatin (SNAP-HP1α) (Videos S2 and S3). Hubs containing dense high-frequency H3.3-SNAP genomic interactions were found within distinct subregions in the nucleus (Fig. 4 *A*, *left panel*). Likewise, heterochromatic hubs harboring high-frequency SNAP-HP1α/chromatin interactions were also observed with similar exchange kinetics, as seen in previous fluorescence recovery after photobleaching studies (Figs. 4 *A*, *right panel*, and S7 *A*) (43,44). Overall, this approach identifies distinct nuclear hubs where proteins associated with euchromatin and heterochromatin dynamically load and unload on the genome in a live cell.

PBAF's stability on euchromatin and heterochromatin is differentially regulated via BAF180 bromodomains

To test if PBAF selectively engages different types of chromatin in hubs, we performed dual-color single-molecule imaging of PBAF (Halo-BAF180) and euchromatin (H3.3-SNAP) or heterochromatin (SNAP-HP1α) in live cells (Videos S4 and S5). WT PBAF and euchromatic/heterochromatic hubs in close proximity (within 500 nm of each hub's centroid position) were identified and further analyzed to determine WT PBAF's chromatin-binding profiles (Fig. 4 *B*). We conservatively chose 500 nm as our limit of co-localization given that our hubs are ∼200–400 nm in diameter. In addition, PBAF and H3.3/HP1α were sequentially imaged ($\Delta t = \sim 20$ min), which may allow chromatin targets in hubs to slightly shift position over our temporal imaging window.

Fitting of PBAF's residence time of co-localization data using a double exponential-decay model indicated no difference in PBAF's stable engagement of chromatin (e.g., percentage of binding events >1 s) in close proximity to euchromatic versus heterochromatic hubs (Fig. 4 *C*). However, GRID analysis, which allows finer partitioning of kinetic species, showed an increase in percentages of WT PBAF molecules that transiently engaged (<1 s binding, P1) chromatin close to heterochromatic versus euchromatic hubs (Fig. 4 *D*). Therefore, PBAF's stable engagement (>1 s, P2/P3/P4) with chromatin in hubs appears to be dependent on the subtypes (e.g., euchromatic versus heterochromatic) of its neighboring chromatin hubs.

When assaying PBAF's stability on a bound nucleosome of different chromatin subtypes, we found that WT PBAF bound chromatin hubs near euchromatic hubs (10.7 s) for significantly less time compared with heterochromatic hubs (15.2 s) using fitting with a double exponential-decay model (Fig. 4 *C*). GRID analysis indicated four WT PBAF chromatin-binding populations near euchromatic hubs and only three WT PBAF chromatin-binding populations near heterochromatic hubs (Fig. 4 *D*). Residence times of the first population (P1, ∼0.7 s) were similar for PBAF bound near euchromatic and heterochromatic hubs (Fig. 4 *D*). The residence time for PBAF bound in the second population (P2) increased ($p < 0.0001$) near heterochromatic (4.7 s) versus euchromatic hubs (3.6 s). The residence time of PBAF's third population (P3) near heterochromatic hubs (25.6 ± 3.1 s) increased ($p < 0.0001$) compared with PBAF's fourth population (P4) near euchromatic hubs (22.4 ± 2.9 s). Overall, our data suggest that PBAF binds differentially (3 versus 4 populations) and longer to chromatin near

A

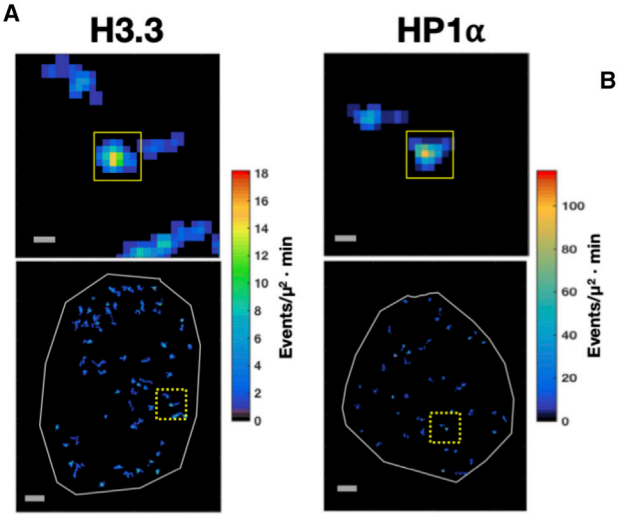

B

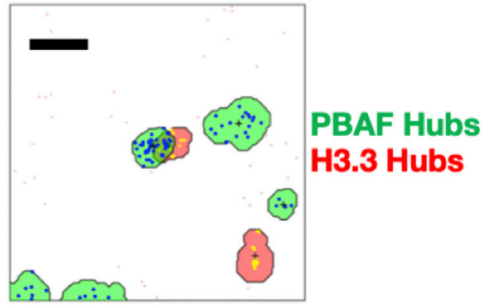

C

	PBAF	Pop_T (%)	Pop_S (%)	τ_T (seconds)	τ_S (seconds)
euchromatin	WT	79.8	20.2	0.90 ± 0.02	10.7 ± 0.42
	ΔBD	82.1	17.9	0.92 ± 0.01	13.1 ± 0.22
heterochromatin	WT	80.4	19.6	0.92 ± 0.03	15.2 ± 0.75
	ΔBD	82.1	17.9	0.87 ± 0.01	11.3 ± 0.34

D

	PBAF	P_1 (%)	τ_1 (s)	P_2 (%)	τ_2 (s)	P_3 (%)	τ_3 (s)	P_4 (%)	τ_4 (s)
Euchromatin (H3.3)	WT	55.2 ±2.2	0.67 ±0.02	29.3 ±6.4	3.6 ±0.4	8.7 ±6.9	7.0 ±1.2	5.2 ±1.3	22.4 ±2.9
	ΔBD	58.8 ±0.7	0.69 ±0.01	30.1 ±1.2	3.7 ±0.2	6.8 ±2.1	11.2 ±2.0	3.4 ±1.6	24.9 ±2.7
Heterochrom. (HP1α)	WT	65.2 ±1.8	0.67 ±0.02	27 ±2.1	4.7 ±0.3	P_3	7.1 ±1.4	τ_3	25.6 ±3.1
	ΔBD	63.7 ±1.0	0.66 ±0.01	28.3 ±1.0	4.0 ±0.2	P_3	7.5 ±0.8	τ_3	15.8 ±1.3

FIGURE 4 Spatial analysis of PBAF chromatin binding activities near H3.3- and HP1α-marked chromatin hubs. (*A*) High frequency binding hubs for H3.3-SNAP (*left panels*) or SNAP-HP1α (*right panels*). Top panels represent an enlarged view of the region outlined in yellow dashed boxes in bottom panels. The nucleus edge is shown in gray. Scale bars, 0.25 μm (*top panel*) and 2 μm (*bottom panel*). (*B*) Representative co-localization of a Halo-BAF180 WT hub (*green hubs with blue binding events*) and H3.3-SNAP hub (*red hubs with yellow binding events*). Scale bar, 0.5 μm. (*C*) Table of the distribution of T and S chromatin residence for WT and ΔBD PBAF near euchromatic and heterochromatic hubs. Median values for the population (Pop) are reported as percentages, while the τ is in seconds. (*D*) Table of GRID analysis for chromatin residence of WT and ΔBD PBAF near euchromatic and heterochromatic hubs. $N = 4673$ WT binding events in 16 WT/H3.3 cells, $N = 28{,}116$ ΔBD binding events in 16 ΔBD/H3.3 cells, $N = 2563$ WT binding events in 15 WT/HP1α cells, and $N = 8859$ ΔBD binding events in 11 ΔBD/HP1α cells. To see this figure in color, go online.

heterochromatic hubs compared with euchromatic hubs. We speculate that PBAF's residence time may be dependent on whether the nucleosome needs to be evicted (transcriptional activation in euchromatin) or mobilized and/or likely stabilized without eviction (transcriptional repression in heterochromatin) (Fig. 6). This data is also consistent with WT

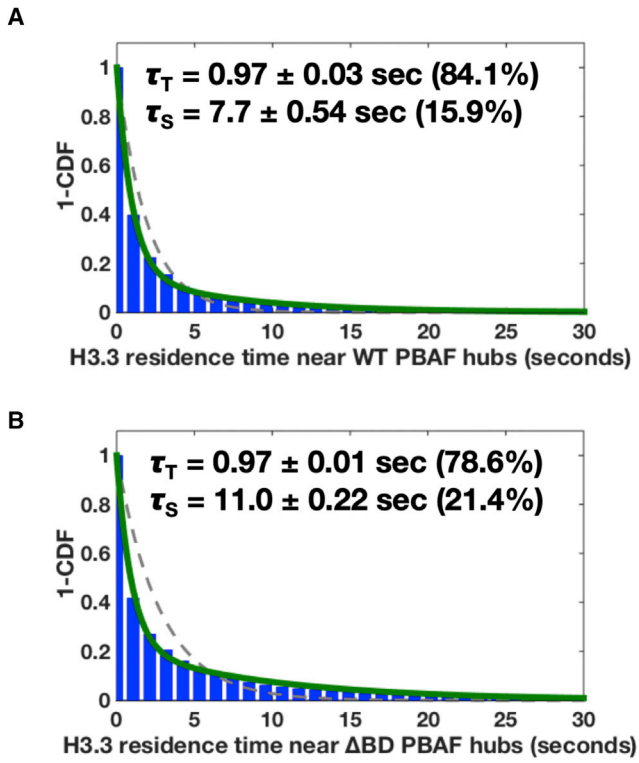

FIGURE 5 Residence-time analysis of H3.3 inside hubs near WT- and ΔBD PBAF-marked chromatin hubs. (*A*) (1-CDF) of H3.3's chromatin-binding τ inside hubs near WT PBAF hubs. (*B*) 1-CDF of H3.3's chromatin-binding τ inside hubs near ΔBD PBAF in a cell. 1-CDF plots were fitted to a single (*dashed gray*) and double (*solid green*) exponential-decay model. The τ and its corresponding percentage for each population (i.e., T and S) are indicated. $N = 2184$ H3.3 binding events in 16 WT/H3.3 cells and $N = 15{,}130$ H3.3 binding events in 16 ΔBD/H3.3 cells. To see this figure in color, go online.

PBAF's enhanced residence time on global chromatin, which is predicted to be more stable and heterochromatic (compare Fig. 3E with Fig. S6 *C*).

Euchromatin is typically acetylation rich. Therefore, we predicted that BAF180 bromodomains would play an important role in stabilizing a PBAF complex bound to euchromatin. However, removal of BAF180 bromodomains led to an enhanced stability (e.g., decreased k_{off}) of ΔBD PBAF bound near H3.3 hubs (e.g., euchromatin) when analyzed using a double exponential-decay model (Fig. 4 *C*). GRID analysis also suggests enhanced stability of ΔBD PBAF bound near H3.3 hubs with increased residence times of P3 (11.2 vs. 7.0 s) and P4 (24.9 vs. 22.6 s) relative to WT PBAF (Fig. 4 *D*).

PBAF's stability on chromatin is likely highly dependent on the ability of PBAF to remodel and evict the nucleosome (Fig. 3 *A*; see discussion). Therefore, it was possible that removal of BAF180 bromodomains effectively slowed down ΔBD PBAF's ability to evict its bound H3.3-containing nucleosome, resulting in an increased chromatin-binding residence time. To test this hypothesis, we examined the residence times of H3.3-SNAP in close proximity (500 nm) to either WT or ΔBD PBAF hubs. Consistent with our model, the stability of H3.3 on chromatin was higher near ΔBD PBAF compared with WT PBAF hubs (Figs. 5 and 6 *A*). Therefore, our data suggest that BAF180 bromodomains may help PBAF to rapidly disassemble or mobilize H3.3-containing nucleosomes.

Residence-time analysis of PBAF indicated that BAF180 bromodomains promoted stabilize engagement (>1 s) of PBAF with global chromatin (Fig. S6 *A* and *C*). This suggests that global chromatin can be acetylated to some degree. Since global chromatin is also likely highly heterochromatic, we compared WT and ΔBD PBAF's stability on chromatin near HP1α hubs (e.g., heterochromatin). We found that ΔBD PBAF near heterochromatic hubs exhibited weakened stability on chromatin compared with WT PBAF via fitting using a double exponential-decay model and GRID analyses (Fig. 4 *C* and *D*). This suggests that BAF180 bromodomains enhance PBAF's stability on heterochromatin, consistent with PBAF's role in stabilizing nucleosomes to repress transcription (20,21) (Fig. 6 *B*). Alternatively, BAF180 bromodomains stabilize PBAF on heterochromatin to help PBAF remodel a more stable nucleosome. To discern between these two possibilities, we measured the residence time of HP1α near WT and ΔBD PBAF hubs. Consistent with our model indicating that bromodomains help PBAF to remodel a nucleosome, the stability of HP1α on chromatin was higher near ΔBD PBAF compared with WT PBAF hubs (Fig. S7 *A*).

To support live-cell dynamic tracking of PBAF binding on select chromatin states, super-resolution STORM microscopy in fixed cells was also conducted (Fig. S8). There appears to be a close association and overlap between WT PBAF and H3.3/HP1α-marked chromatin (Fig. S8, *magenta*). In many subnuclear regions, PBAF binds chromatin and forms a distinct close interface surrounding H3.3-marked chromatin domains (Fig. S8, *bottom left panel*, *highlighted in magenta*), consistent with the results in Fig. 4 *B*. A similar but less pronounced pattern was seen with PBAF- and HP1α-marked chromatin domains (Fig. S8, *bottom right panel*). Taken together, these studies illustrate that PBAF can selectively bind distinct types of chromatin via BAF180's bromodomains.

DISCUSSION

A battery of live-cell single-molecule and luciferase-based imaging studies have now established that transcription is a stochastic process consisting of short bursts of transcription (minutes) intervened by periods of inactivity (minutes to hours) (45,46). Transitions between transcriptionally active and inactive genes are likely accompanied by the surrounding chromatin interchanging between euchromatin and heterochromatin, respectively (3). These transitions are likely driven by dynamic transcription-factor binding accompanied by DNA looping, allowing transient interactions between enhancers and promoters (47). Accordingly, this cyclical nature

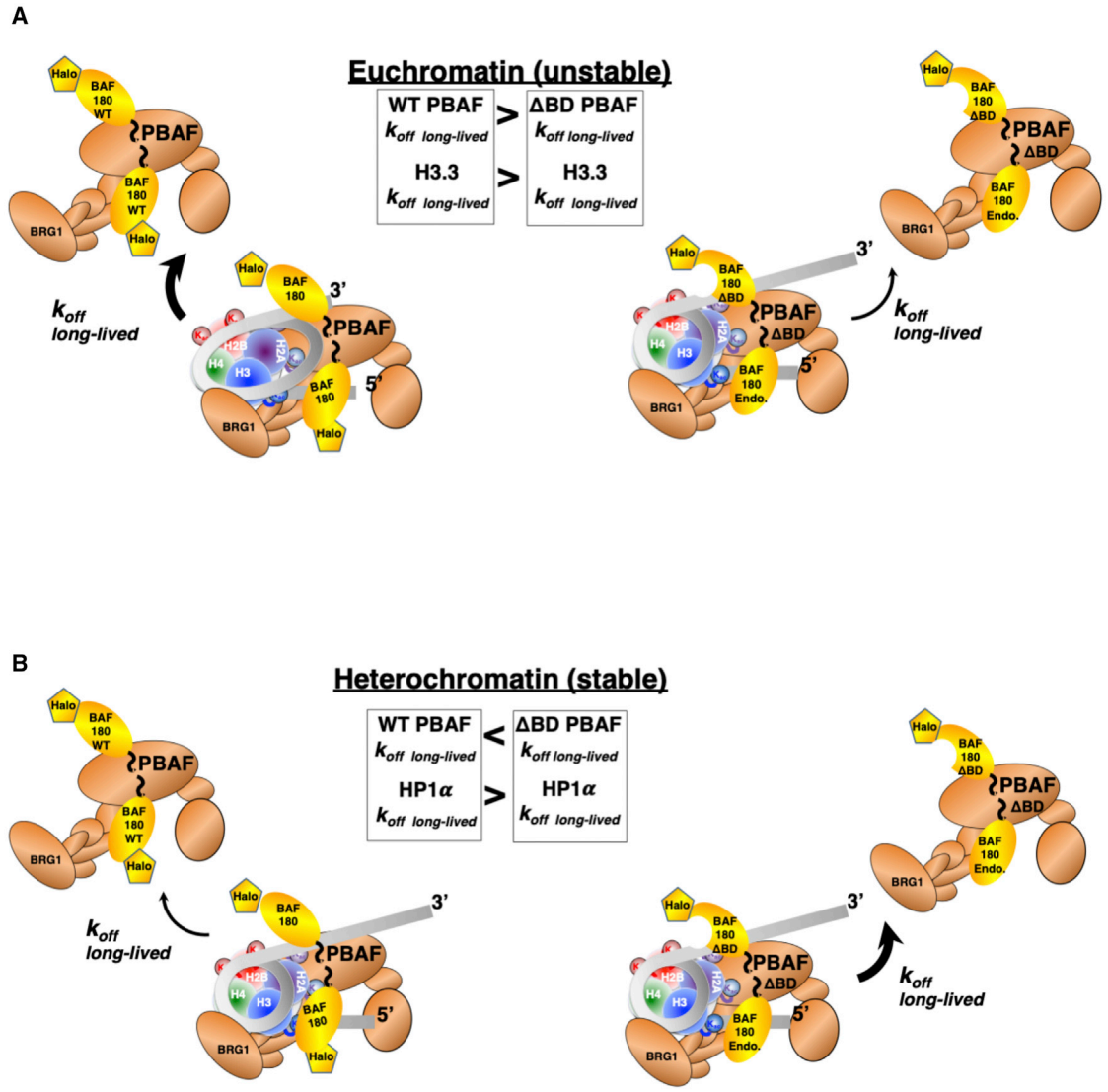

Figure360▷ FIGURE 6 For a Figure360 author presentation of Fig. 6, see https://doi.org/10.1016/j.bpj.2022.03.027.
Putative models of PBAF's dynamic chromatin binding to different chromatin states. (*A*) In euchromatin, PBAF's main role is to evict or move nucleosomes to allow access of transcription factors to genomic sites. In this scenario, PBAF's τ may be affected by the nucleosome stability. Removal of six bromodomains in one copy of BAF180 (*right*) stabilizes PBAF on euchromatin (decreased $k_{off\ long\text{-}lived}$), potentially by impacting its ability to remodel the nucleosome. H3.3's τ is related to PBAF's τ. (*B*) PBAF fundamentally interacts with heterochromatin differently than euchromatin. In this scenario, PBAF remains bound to heterochromatin for longer periods of time (decreased $k_{off\ long\text{-}lived}$) due to BAF180 bromodomain-mediated contacts with the nucleosome (*left*). HP1α may bind for longer due to enhanced contacts with H3K9me3 in the absence of six bromodomains in one copy of BAF180 (*right*). In this model, $k_{off\ long\text{-}lived}$ represents τ in PBAF/H3.3/HP1α chromatin-binding populations lasting longer than ∼3–4 s. To see this figure in color, go online.

of going from active to inactive gene states suggests that chromatin-remodeling enzymes, chromatin-bound factors, histones, and transcription factors dynamically bind and unbind chromatin at highly select regions of the nucleus over relatively short timescales. Indeed, our imaging data indicates that PBAF, H3.3, and HP1α can be added to the growing list of transcription factors (RNA Pol II, mediator, EWS/FLI, and Sox2) that have been shown to form hubs or clusters in live cells (7–11). Our imaging studies also show distinct differences in PBAF's engagement and chromatin-binding residence time inside and outside (Figs. 3 *D*, *E*, S5, and S6) of hubs, further validating our hub-calling approach. Therefore, we and other research groups have established that dynamic SMT is useful for identifying and characterizing chromatin binding of a broad range of nuclear factors in hubs of activity (11,12).

However, little is known about how chromatin hubs are dynamically targeted and bound by chromatin remodelers. Using dynamic live-cell SMT, chromatin-binding-frequency heatmaps allowed us to visualize PBAF binding to chromatin hubs. We propose that the discrete PBAF hubs identified in our heatmaps (Fig. 1 *D*) represent repeated binding to arrays

of closely spaced acetylated nucleosomes likely present in enhancers and promoters during our live-cell imaging (Fig. 2). Based upon our data, spatial confinement of PBAF hubs over a small region of the nucleus (200–400 nm) may also suggest that the genomic scaffold of chromatin targets does not move appreciable over our 18 min imaging window. Albeit, there may be long-range dynamic enhancer/promoter DNA looping that occurs during this time frame.

Removal of BAF180's bromodomains reduced the number of ΔBD PBAF hubs, while elevated global histone acetylation increased the number of hubs for WT PBAF (Figs. 2 *C* and S4 *C*). Removal of BAF180 bromodomains did not completely eliminate ΔBD PBAF targeting to hubs (Fig. 2 *C*). Therefore, PBAF may utilize bromodomains in its BRD7/BRG1 subunits to target select BAF180-independent chromatin hubs. PBAF may also use additional chromatin-binding domains (PHD and/or BAH domains) for engagement of BAF180-independent chromatin hubs. Alternatively, the one copy of endogenous BAF180 that contains bromodomains in our ΔBD PBAF complex (Fig. S1 *C* and *D*) may suffice to target the mutant PBAF to chromatin hubs.

Temporal analysis of PBAF binding to chromatin in a hub revealed rapid on and off binding cycles (Fig. 2 *D*) that may be expected if PBAF was remodeling nucleosomal arrays. Deletion of BAF180 bromodomains weakened the efficiency of PBAF's stable engagement of chromatin by reducing the percentage of ΔBD PBAF lasting longer than 1 s (e.g., stably bound) (Fig. 3 *D* and *E*). This suggests that BAF180 bromodomains play a critical role in PBAF's productive association (stable k_{engage}) with chromatin that would be required for PBAF to rapidly bind and unbind to potentially remodel neighboring nucleosomes in an array (Figs. 2 *A* and 3 *A*).

Based on in vitro experiments, PBAF's binding to acetylated chromatin is stabilized by BAF180 bromodomains (16,17). However, these in vitro experiments were performed in the absence of ATP, which prevents PBAF from evicting the nucleosome from DNA. Our live-cell imaging studies are measuring PBAF's chromatin-binding and remodeling activity in the presence of ATP. Therefore, PBAF's chromatin-binding residence time in vivo depends on the strength of its interactions with a nucleosome and the overall stability of the nucleosome once ATP hydrolysis begins to initiate remodeling. Although we have not measured PBAF-mediated chromatin remodeling in live cells, we hypothesize that PBAF's ability to remodel a nucleosome will affect its residence time on chromatin. This idea is also supported by SMT studies of yeast ATP-dependent chromatin remodelers where inactivation of enzymatic activity increased chromatin-binding residence times by roughly twofold, as discussed further below (33). Therefore, ATP-dependent remodeling activity decreases chromatin-binding stability of multiple chromatin remodelers, including RSC, which is the yeast homolog of PBAF.

Our imaging experiments revealed that PBAF displayed shorter chromatin-binding residence times near H3.3-marked euchromatic hubs, which should be more easily mobilized and/or evicted compared with HP1α-containing nucleosomes in heterochromatic hubs, which should be less easily removed (Fig. 4 *C* and *D*). This is consistent with in vitro and in vivo studies showing an inherent instability of H3.3-containing nucleosomes (48–51). Due to technical limitations, we are not yet able to directly measure PBAF-mediated nucleosome eviction. However, we speculate that the rapid turnover of PBAF's chromatin occupancy near euchromatin may potentially be affected by nucleosome stability or remodeling potential, which helps to define different chromatin states (Fig. 6).

Contrary to the dogma of in vitro experiments, removal of BAF180 bromodomains increased ΔBD PBAF's chromatin-binding residence time near euchromatic hubs, as seen with multiple fitting techniques (Fig. 4 *C* and *D*). Based upon this result, we speculate that ΔBD PBAF's increased chromatin residence time may be a reflection of a slower rate of nucleosome mobilization and/or eviction. Indeed, our experiments showed that H3.3 is stabilized in chromatin when BAF180 bromodomains are removed (Fig. 4 *E*). This is consistent with a previous in vitro biochemical study comparing the remodeling activity of RSC, the yeast homolog of PBAF that contains multiple bromodomains, versus SWI/SNF, a highly related complex with only a single bromodomain (34). RSC stimulated nucleosome movement and H2A/H2B dimer displacement more than SWI/SNF in an H3 acetyl-dependent manner (34). Removal of the lone bromodomain in SWI/SNF also decreased nucleosome movement and H2A/H2B dimer displacement in an acetylation-dependent manner. Together, these results suggest that bromodomains within RSC may help speed nucleosome movement and H2A/H2B dimer displacement. Based upon our live-cell measurements and this prior in vitro experiment, we speculate that removal of BAF180 bromodomains may be converting WT PBAF into a complex that moves and/or evicts nucleosomes at a slower rate.

Previous studies indicated that PBAF regulates transcriptional repression, suggesting that PBAF also binds heterochromatin via an unknown mechanism (18–21). Our live-cell and STORM imaging data (Figs. 4 *C*, *D*, and S8) directly supports this premise that PBAF engages heterochromatin. Importantly, both WT and ΔBD PBAF's interaction with heterochromatin and euchromatin differed when comparing the number of binding populations and residence times (Fig. 4 *C* and *D*). This suggests that PBAF fundamentally interacts differently with heterochromatin compared with euchromatin. We speculate that this differential interaction depends on BAF180 bromodomains since ΔBD PBAF resides on chromatin near heterochromatic hubs for shorter periods of time compared with WT PBAF.

It is unknown how BAF180 bromodomains engage with heterochromatin that is typically envisioned to be deficient in acetylated histones. However, previous mass-spectrometry studies have shown that chromatin contains bivalent modifications such as H3K9me3/H3K14ac on the same nucleosome

(52,53). We speculate that PBAF may recognize H3K9me3/H3K14ac in our HP1α-marked heterochromatic regions given that HP1α binds H3K9me3 and the BAF180/BRG1 subunits interact with H3K14ac (27). To increase PBAF's stability on heterochromatin, it is possible that PBAF simultaneously binds the H3K9me3/H3K14ac mark via the PHF10 PHD finger and the BAF180 bromodomains, respectively. Competition between PBAF and HP1α for H3K9me3/H3K14ac is supported by our data showing that removal of BAF180 bromodomains increased the stability of HP1α on chromatin (Fig. S7 *A*).

Additional future studies investigating the interaction of PHF10 and BAF180 with distinct chromatin marks inside cells should help test this hypothesis and further define PBAF's engagement with heterochromatin.

Single-molecule residence times have typically been interpreted to reflect binding affinities of transcription factors on target sites in chromatin. However for ATP-dependent chromatin-remodeling enzymes like PBAF, a residence time is likely the time that it takes to evict/move a nucleosome, which is PBAF's main role in vivo. In this regard, a reduction in PBAF's enzymatic activity would decrease the rate of nucleosome eviction, allowing PBAF to bind nucleosomes for a much longer time and thus lead to an increase in residence time. Indeed, a recent SMT study showed that enzymatic inactivation of the ATPase domain increased the residence time of multiple mutant chromatin-remodelers by at least twofold (33).

This concept is also consistent with our previous study showing that mutational inactivation of DNA polymerase activity increased chromatin-binding residence times in vivo (28). This general phenomenon is likely due to the fact that an enzyme's affinity for targets evolved to bind as long as it takes to exert its catalytic activity. However, when catalytic activity is inhibited, there is likely an upper time limit for substrate engagement leading to dissociation so that another enzyme can now attempt to utilize the substrate for catalysis.

CONCLUSIONS

By characterizing the dynamic chromatin binding of PBAF and a bromodomain mutant on different types of chromatin, our work helps to define the spatial and temporal changes of chromatin states. Future live-cell single-molecule imaging studies of additional ATP-dependent chromatin remodelers along with histone PTM writers and readers and the histone marks themselves will shine new light on the spatiotemporal organization of the 4D epigenome.

DATA AVAILABILITY

SPT datasets (accession number 4DNES2DS2N1U) can be found at the NIH 4DN Data Portal (https://data.4dnucleome.org). "NIH 4DN Data Portal: https://data.4dnucleome.org/experiment-set-replicates/4DNES2DS2N1U/".

SUPPORTING MATERIAL

Supporting material can be found online at https://doi.org/10.1016/j.bpj.2022.03.027.

AUTHOR CONTRIBUTIONS

Designed and supervised experiments, R.A.C., C.A.K., S.-H.L., P.C., W.-L.L., N.H., and R.H.S.; generated material, C.A.K. (cell lines, constructs), V.W. (cell lines, constructs), P.D. (cell lines), and L.D.L. (JF dyes); performed experiments, C.A.K., P.C., V.W., and N.H.; analyzed data, C.A.K., S.-H.L., P.C., V.W., R.A.C., and W.-L.L.; wrote paper, R.A.C., W.-L.L., and C.A.K.

ACKNOWLEDGMENTS

We thank Y.J. Chen and C.S. Peng for development of initial Matlab scripts used for SMT tracking. We are grateful to Z. Liu (Janelia Research Campus) for providing the Matlab script and for technical advice on the analysis of diffusion rates and paired-correlation analysis. We thank S. Healton for reagents and technical assistance in acid extraction of histones and J.C. Wheat for providing suberoylanilide hydroxamic acid reagent and initial aliquots of acetyl-H3 antibody. We also thank D. Shechter for providing the histone H3 antibody. We also thank the NHLBI imaging facility for allowing us to use their STORM imaging system. This work was supported by a grant from the NIH (8U01DA047729-04, R.A.C. and R.H.S.) as part of the 4D Nucleome project, the NIH (1R01GM126045-01, R.A.C.), and a NIH Medical Scientist Training Program Grant (T32GM007288, C.A.K.).

REFERENCES

1. Tantale, K., F. Mueller, …, E. Bertrand. 2016. A single-molecule view of transcription reveals convoys of RNA polymerases and multi-scale bursting. *Nat. Commun.* 7:12248.
2. Biswas, J., W. Li, …, R. A. Coleman. 2021. Imaging organization of RNA processing within the nucleus. *Cold Spring Harbor Perspect. Biol.* 13:a039453.
3. Allis, C. D., and T. Jenuwein. 2016. The molecular hallmarks of epigenetic control. *Nat. Rev. Genet.* 17:487–500.
4. Henikoff, S., E. McKittrick, and K. Ahmad. 2004. Epigenetics, histone H3 variants, and the inheritance of chromatin states. *Cold Spring Harbor Symp. Quant. Biol.* 69:235–243.
5. McKittrick, E., P. R. Gafken, …, S. Henikoff. 2004. Histone H3.3 is enriched in covalent modifications associated with active chromatin. *Proc. Natl. Acad. Sci. U S A.* 101:1525–1530.
6. Eissenberg, J. C., and S. C. Elgin. 2014. HP1a: a structural chromosomal protein regulating transcription. *Trends Genet.* 30:103–110.
7. Cho, W. K., N. Jayanth, …, I. I. Cisse. 2016. RNA Polymerase II cluster dynamics predict mRNA output in living cells. *eLife.* 5:e13617.
8. Cisse, I. I., I. Izeddin, …, X. Darzacq. 2013. Real-time dynamics of RNA polymerase II clustering in live human cells. *Science.* 341:664–667.
9. Liu, Z., W. R. Legant, …, R. Tjian. 2014. 3D imaging of Sox2 enhancer clusters in embryonic stem cells. *Elife.* 3:e04236.
10. Cho, W. K., J. H. Spille, …, I. I. Cisse. 2018. Mediator and RNA polymerase II clusters associate in transcription-dependent condensates. *Science.* 361:412–415.
11. Chong, S., C. Dugast-Darzacq, …, R. Tjian. 2018. Imaging dynamic and selective low-complexity domain interactions that control gene transcription. *Science.* 361:eaar2555.
12. Mir, M., A. Reimer, …, X. Darzacq. 2017. Dense Bicoid hubs accentuate binding along the morphogen gradient. *Genes Dev.* 31:1784–1794.

13. Porter, E. G. 2019. PBRM1 regulates stress response in epithelial cells. *iScience.* 15:196–210.
14. Kuzmanov, A., E. I. Karina, …, D. S. Fay. 2014. The conserved PBAF nucleosome-remodeling complex mediates the response to stress in Caenorhabditis elegans. *Mol. Cell Biol.* 34:1121–1135.
15. Damelin, M., I. Simon, …, P. A. Silver. 2002. The genome-wide localization of Rsc9, a component of the RSC chromatin-remodeling complex, changes in response to stress. *Mol. Cell.* 9:563–573.
16. Porter, E. G., and E. C. Dykhuizen. 2017. Individual bromodomains of polybromo-1 contribute to chromatin association and tumor suppression in clear cell renal carcinoma. *J. Biol. Chem.* 292:2601–2610.
17. Slaughter, M. J., E. K. Shanle, …, I. J. Davis. 2018. PBRM1 bromodomains variably influence nucleosome interactions and cellular function. *J. Biol. Chem.* 293:13592–13603.
18. Mashtalir, N., A. R. D'Avino, …, C. Kadoch. 2018. Modular organization and assembly of SWI/SNF family chromatin remodeling complexes. *Cell.* 175:1272–1288.e20.
19. Moreira, J. M., and S. Holmberg. 1999. Transcriptional repression of the yeast CHA1 gene requires the chromatin-remodeling complex RSC. *EMBO J.* 18:2836–2844.
20. Lee, H., F. Dai, …, B. Gan. 2016. BAF180 regulates cellular senescence and hematopoietic stem cell homeostasis through p21. *Oncotarget.* 7:19134–19146.
21. Wurster, A. L., P. Precht, …, M. J. Pazin. 2012. IL-10 transcription is negatively regulated by BAF180, a component of the SWI/SNF chromatin remodeling enzyme. *BMC Immunol.* 13:9.
22. Serge, A., N. Bertaux, …, D. Marguet. 2008. Dynamic multiple-target tracing to probe spatiotemporal cartography of cell membranes. *Nat. Methods.* 5:687–694.
23. Normanno, D., L. Boudarene, …, M. Dahan. 2015. Probing the target search of DNA-binding proteins in mammalian cells using TetR as model searcher. *Nat. Commun.* 6:7357.
24. Chen, J., Z. Zhang, …, Z. Liu. 2014. Single-molecule dynamics of enhanceosome assembly in embryonic stem cells. *Cell.* 156:1274–1285.
25. Ricci, M. A., C. Manzo, …, M. P. Cosma. 2015. Chromatin fibers are formed by heterogeneous groups of nucleosomes in vivo. *Cell.* 160:1145–1158.
26. Roh, T. Y., S. Cuddapah, and K. Zhao. 2005. Active chromatin domains are defined by acetylation islands revealed by genome-wide mapping. *Genes Dev.* 19:542–552.
27. Charlop-Powers, Z., L. Zeng, …, M. M. Zhou. 2010. Structural insights into selective histone H3 recognition by the human Polybromo bromodomain 2. *Cell Res.* 20:529–538.
28. Drosopoulos, W. C., D. A. Vierra, …, C. L. Schildkraut. 2020. Dynamic assembly and disassembly of the human DNA polymerase delta holoenzyme on the genome in vivo. *Cell Rep.* 30:1329–1341.e5.
29. Hassan, A. H., P. Prochasson, …, J. L. Workman. 2002. Function and selectivity of bromodomains in anchoring chromatin-modifying complexes to promoter nucleosomes. *Cell.* 111:369–379.
30. Ho, L., and G. R. Crabtree. 2010. Chromatin remodelling during development. *Nature.* 463:474–484.
31. Brownlee, P. M., A. L. Chambers, …, J. A. Downs. 2012. Cancer and the bromodomains of BAF180. *Biochem. Soc. Trans.* 40:364–369.
32. Filippakopoulos, P., S. Picaud, …, S. Knapp. 2012. Histone recognition and large-scale structural analysis of the human bromodomain family. *Cell.* 149:214–231.
33. Kim, J. M., P. Visanpattanasin, …, C. Wu. 2021. Single-molecule imaging of chromatin remodelers reveals role of ATPase in promoting fast kinetics of target search and dissociation from chromatin. *Elife.* 10:e69387.
34. Chatterjee, N., D. Sinha, …, B. Bartholomew. 2011. Histone H3 tail acetylation modulates ATP-dependent remodeling through multiple mechanisms. *Nucleic Acids Res.* 39:8378–8391.
35. Zhang, Y., C. L. Smith, …, C. Bustamante. 2006. DNA translocation and loop formation mechanism of chromatin remodeling by SWI/SNF and RSC. *Mol. Cell.* 24:559–568.
36. Harada, B. T., W. L. Hwang, …, X. Zhuang. 2016. Stepwise nucleosome translocation by RSC remodeling complexes. *Elife.* 5:e10051.
37. Coleman, R. A., Z. Liu, …, T. Lionnet. 2016. Imaging transcription: past, present, and future. *Cold Spring Harbor Symp. Quant. Biol.* 80:1–8.
38. Reisser, M., J. Hettich, …, J. C. M. Gebhardt. 2020. Inferring quantity and qualities of superimposed reaction rates from single molecule survival time distributions. *Sci. Rep.* 10:1758.
39. Popp, A. P., J. Hettich, and J. C. M. Gebhardt. 2021. Altering transcription factor binding reveals comprehensive transcriptional kinetics of a basic gene. *Nucleic Acids Res.* 49:6249–6266.
40. Kaeser, M. D., A. Aslanian, …, B. M. Emerson. 2008. BRD7, a novel PBAF-specific SWI/SNF subunit, is required for target gene activation and repression in embryonic stem cells. *J. Biol. Chem.* 283:32254–32263.
41. Kakarougkas, A., A. Ismail, …, J. Downs. 2014. Requirement for PBAF in transcriptional repression and repair at DNA breaks in actively transcribed regions of chromatin. *Mol. Cell.* 55:723–732.
42. Van de Vosse, D. W., Y. Wan, …, R. Wozniak. 2013. A role for the nucleoporin Nup170p in chromatin structure and gene silencing. *Cell.* 152:969–983.
43. Cheutin, T., A. J. McNairn, …, T. Misteli. 2003. Maintenance of stable heterochromatin domains by dynamic HP1 binding. *Science.* 299:721–725.
44. Meshorer, E., D. Yellajoshula, …, T. Misteli. 2006. Hyperdynamic plasticity of chromatin proteins in pluripotent embryonic stem cells. *Dev. Cell.* 10:105–116.
45. Shav-Tal, Y., R. H. Singer, and X. Darzacq. 2004. Imaging gene expression in single living cells. *Nat. Rev. Mol. Cell Biol.* 5:855–861.
46. Suter, D. M., N. Molina, …, F. Naef. 2011. Mammalian genes are transcribed with widely different bursting kinetics. *Science.* 332:472–474.
47. Vermunt, M. W., D. Zhang, and G. A. Blobel. 2019. The interdependence of gene-regulatory elements and the 3D genome. *J. Cell Biol.* 218:12–26.
48. Deaton, A. M., M. Gomez-Rodriguez, …, R. E. Kingston. 2016. Enhancer regions show high histone H3.3 turnover that changes during differentiation. *Elife.* 5:e15316.
49. Henikoff, S., J. G. Henikoff, …, K. Ahmad. 2009. Genome-wide profiling of salt fractions maps physical properties of chromatin. *Genome Res.* 19:460–469.
50. Jin, C., and G. Felsenfeld. 2007. Nucleosome stability mediated by histone variants H3.3 and H2A.Z. *Genes Dev.* 21:1519–1529.
51. Jin, C., C. Zang, …, G. Felsenfeld. 2009. H3.3/H2A.Z double variant-containing nucleosomes mark 'nucleosome-free regions' of active promoters and other regulatory regions. *Nat. Genet.* 41:941–945.
52. Jurkowska, R. Z., S. Qin, …, A. Jeltsch. 2017. H3K14ac is linked to methylation of H3K9 by the triple Tudor domain of SETDB1. *Nat. Commun.* 8:2057.
53. Price, A. J., M. C. Manjegowda, …, I. M. Bochkis. 2020. Hdac3, Setdb1, and Kap1 mark H3K9me3/H3K14ac bivalent regions in young and aged liver. *Aging Cell.* 19:e13092.